Electronic Supplementary Material (ESI) for Nanoscale.

Supporting Information: Role of the Cu Substrate in the Growth of Ultra-Flat Crack-Free Highly-Crystalline Single-Layer Graphene

Benjamin Huet* and Jean-Pierre Raskin

Institute of Information and Communication Technologies, Electronics and Applied Mathematics (ICTEAM), Université catholique de Louvain (UCL), Belgium

E-mail: benjamin.huetb@gmail.com

*To whom correspondence should be addressed

S1: Surface roughness and polishing

Cu foils

The surface roughness presented in the core of the paper has been estimated using contact profilometry (Veeco Dektak 150) and atomic force microscopy (Dimension Icon Instrument, Bruker). The profilometry data was acquired using a stylus radius of 2.5 micrometer, a vertical force of 3 mg and a scanning length varying in the 100-500 µm range. The AFM measurements were collected using tapping mode in air, with a linear scanning rate set between 0.5 and 1 Hz. The applied force has been adjusted in the 5-100 nN range depending on the measured surface area (ranging from $50 \times 50\,\mu m^2$ down to $500 \times 500\,nm^2$).

Cu surface roughness data presented in Fig.1 of the paper has been estimated using profilometer data for Cu foils, profilometer and AFM images for polycrystalline Cu films, and exclusively AFM images for epitaxial Cu films. Cu foils exhibit long-range surface morphology changes as the lateral size of Cu grains can reach a few hundreds of micrometers. Using a scanning length of at least 100 µm is thus necessary to go across a few Cu grain boundary grooves and obtain a good estimation of the surface roughness. For polycrystalline Cu films, $50 \times 50\,\mu m^2$ AFM images provide an estimation of the Cu surface roughness which is very close to the one extracted from 100 µm-long profilometer scan because thin polycrystalline films exhibit Cu grains with a lateral size of about 20 micrometers. For epitaxial Cu films, the terraces and step edges represent the major contribution to the Cu surface roughness (in the case of an appropriate CVD process). These terraces usually have a maximum length of 10 microns and the steps have a maximum height of a few nanometers. $50 \times 50\,\mu m^2$ AFM images have thus been used to obtain an estimation of the surface roughness. The error bars indicate the deviation of the roughness measured in at least 5 different locations on each sample.

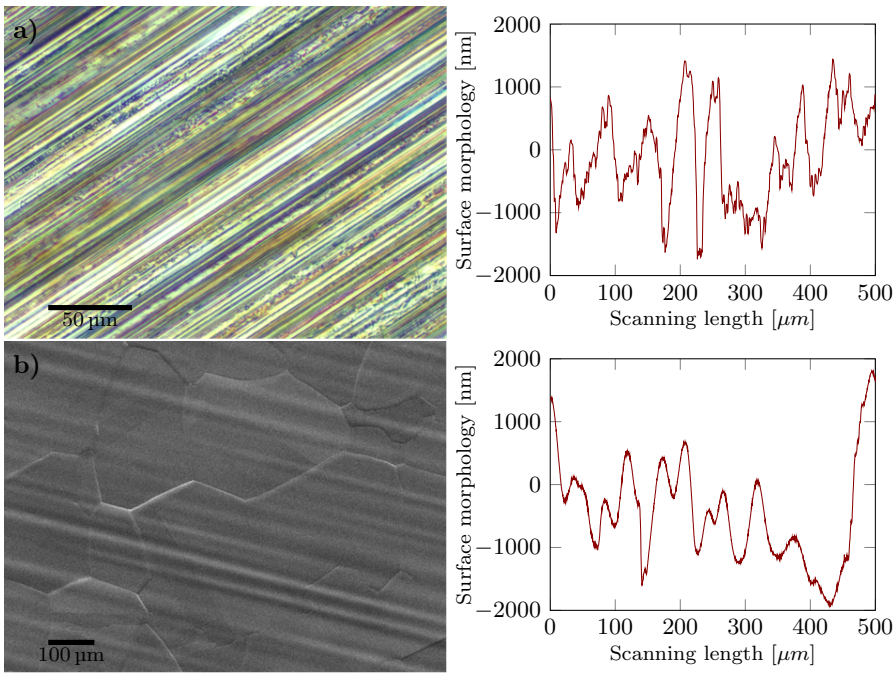

Figure 1: a) DIC optical microscope image taken on the surface of an as-received Cu foil. b) SEM image taken on the surface of a Cu foil annealed for 6 hours at 1050°C under 1000 mbar of Ar/H_2 (10%). Right panel: corresponding typical profilometer scans.

Cold rolling striations are the predominant surface feature on as-received Cu foils (see Fig. 1a). Long duration Cu annealing at high temperature smoothens the Cu surface by suppressing micro-scale Cu surface features but does not remove the striations as shown in the profilometer scans in Fig. 1.

The chemical mechanical polishing employed here consists of two successive steps: the diamond polishing and the oxide polishing. The diamond polishing (MD-mol surface, DiaPro Mol R3, 3-µm-large diamonds, 150 rpm, 10 min) and oxide polishing (MD-Chem surface, OP-S NonDry, 0.04-µm-large silica grains, 150 rpm, 4 min) steps have been achieved using Struers (FR) materials. This procedure greatly improves the surface morphology as it removes cold-rolling striations but leaves very fine scratches on the Cu surface (see Fig. 2a). These scratches vanish after annealing the Cu foil for 1 hour at 1050 °C under ambient pressure conditions (see Fig. 2b).

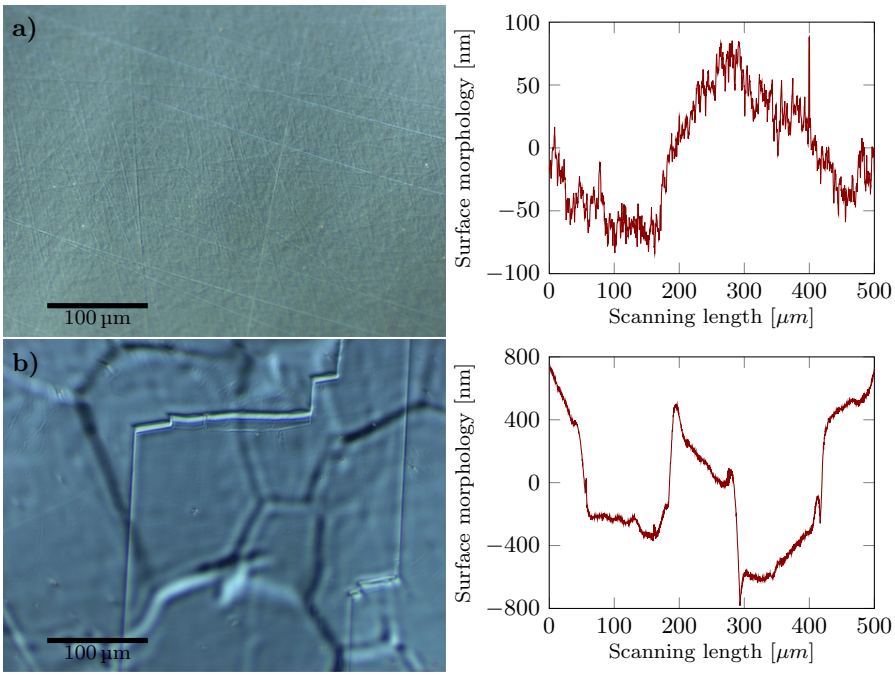

Figure 2: DIC optical microscope images taken on the surface of a Cu foil polished by CMP (a) before and (b) after a CVD process comprising a 1 hour-long graphene growth step at 1050°C under atmospheric pressure conditions. Right panel: corresponding typical profilometer scans.

On polished Cu foils, Cu grain boundary grooves represent the major contributions to the Cu surface roughness.

Cu films

Figures 3 shows that increasing the Cu film thickness significantly affects the Cu grain size and the depths of Cu grain boundary grooves. The profilometer tip dimension is however too large to really reach the bottom of the Cu grain boundary grooves and provide a decent estimation of the depth of the grooves.

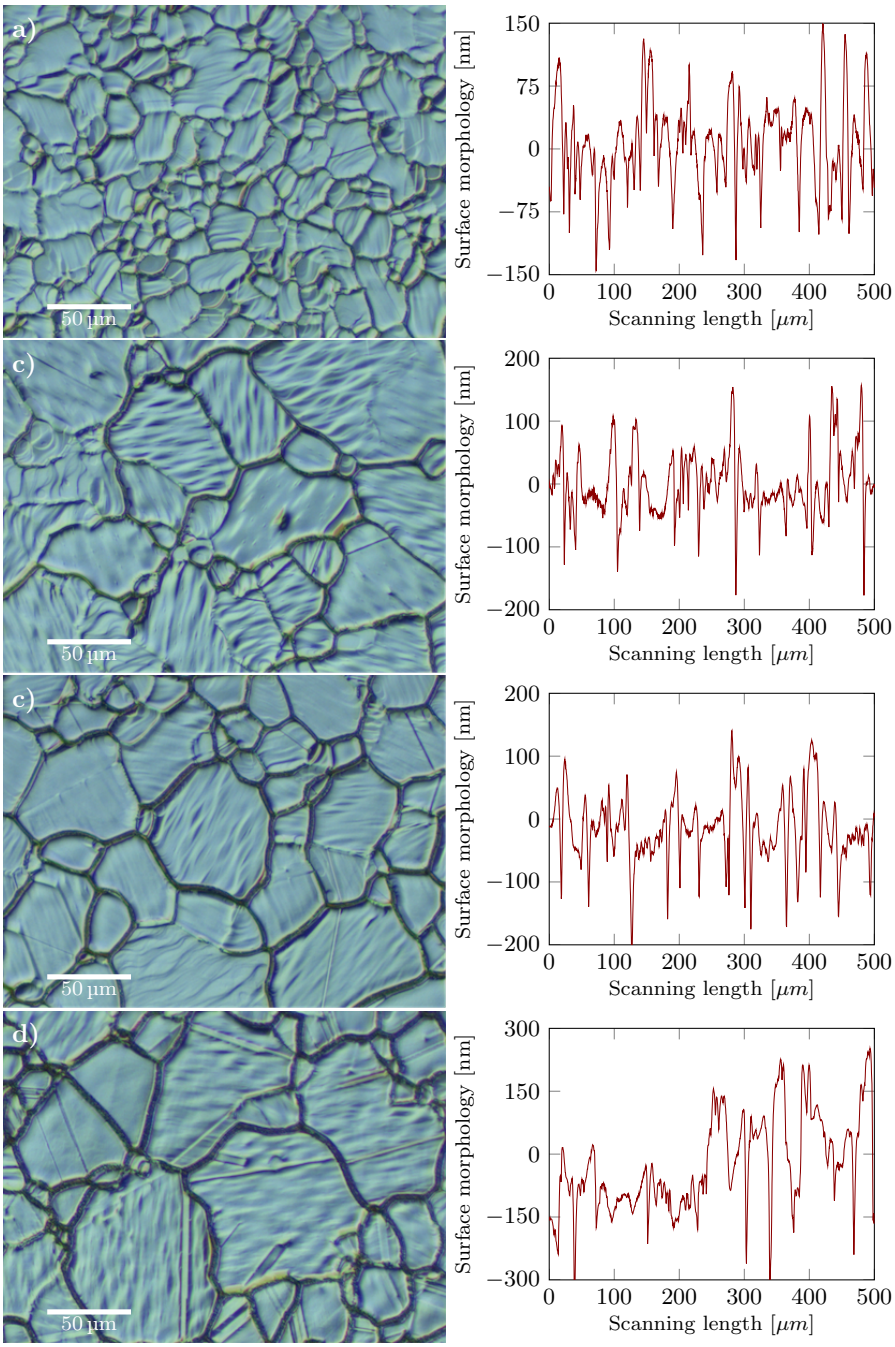

Figure 3: DIC optical microscope images taken on the surface of Cu films with a thickness of (a) 800 nm, (b) 1600 nm, (c) 2400 nm, and (d) 4800 nm after a CVD process comprising a 90 min-long graphene growth step at 1050°C under atmospheric pressure conditions. Right panel: corresponding typical profilometer scans.

A better insight about the surface roughness is obtained using AFM. Figures 4 and 5 show AFM measurements performed on the surface of 800 nm-thick and 4800 nm-thick Cu films after graphene growth, respectively.

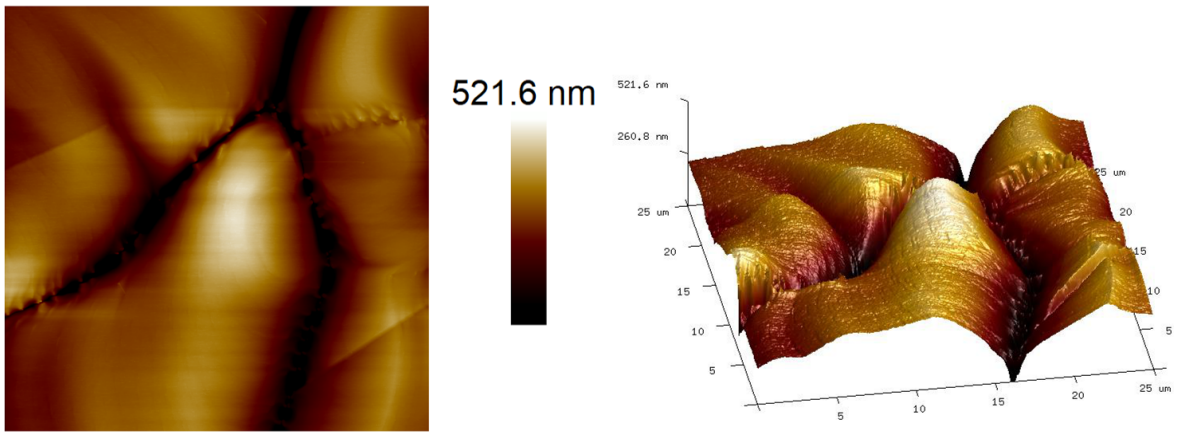

Figure 4: 2D and 3D AFM images of the Cu surface of a 800 nm-thick Cu film (deposited on fused quartz) that has been annealed at 1050°C for 90 min. Grain boundary grooves reach in this case a depth of about 500 nm. The root mean squared and arithmetic surface roughnesses for this AFM image are 84.1 nm and 63.1 nm, respectively. AFM lateral dimensions are $25 \times 25\,\mu m^2$.

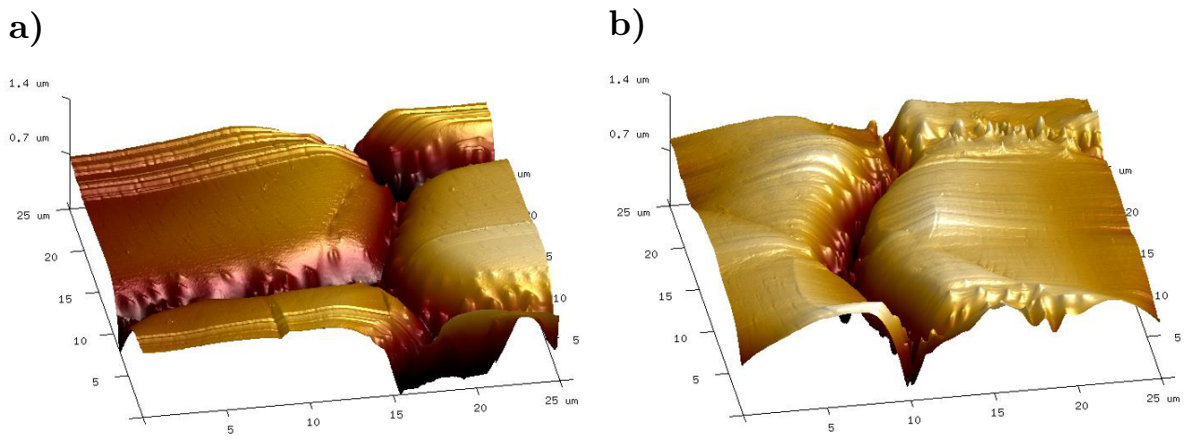

Figure 5: 3D AFM images of the Cu surface acquired in two different locations of a 4800 nm-thick Cu film (deposited on fused quartz) that has been annealed at 1050°C for 90 min. Grain boundary grooves reach in this case a depth of about 1400 nm. The root mean squared and arithmetic surface roughnesses are 149 nm and 110 nm for the AFM image in (a), and 161 nm and 117 nm for the AFM image in (b), respectively.

The projected surface area of each AFM image displayed in Figs. 4, 5 and 6 are 625 μm^2, 625 μm^2 and 1600 μm^2, respectively. The actual AFM surface area however strongly varies with the Cu surface roughness. The image surface area difference is directly related to the amount of wrinkles, cracks and strain that will be generated into the graphene sheet once it is transferred on a device-compatible smooth and flat substrate. Table 1 summarizes the actual surface areas and surface areas difference for each AFM image displayed in Figs. 4, 5 and 6.

Table 1 thus shows that Cu/sapphire substrates have a superior surface roughness compared to other catalysts. As a consequence, transferring graphene from such substrate will offer improved results in terms of graphene physical integrity and strain.

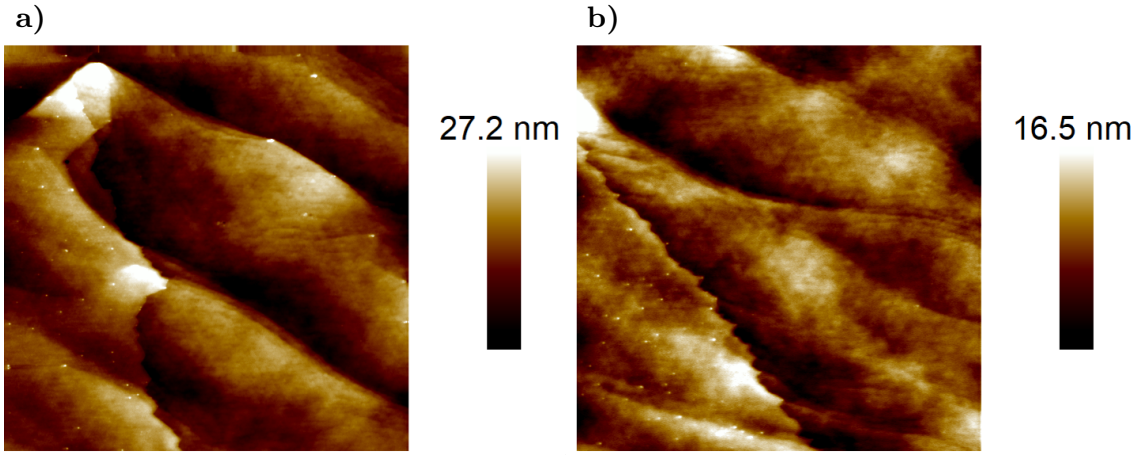

Figure 6: 40×40 µm^2 2D images of the Cu surface of a 1200nm-thick Cu film (deposited on C-plane sapphire) after a CVD process consisting of a 90 min-long graphene growth step at 1050°C. Both AFM images have been taken in the vicinity of a graphene domain edge (graphene is on the right of each image). As Cu grain boundaries are absent, steps-terraces structures represent the major contributor to the Cu surface roughness. The root mean squared and arithmetic surface roughnesses are 5.19 nm and 4.20 nm for the AFM image (a), and 2.91 nm and 2.28 nm for the AFM image (b), respectively.

Table 1: Table summarizing the arithmetic average roughness R_a, the root mean squared roughness R_q, the actual AFM image Cu surface area, and the difference with the projected surface area for the AFM images presented in Figs. 4, 5 and 6.

AFM images	R_q	R_a	Surf. area [µm^2]	surf. area diff.
800 nm Cu/quartz (Fig. 4)	84.1 nm	63.1 nm	631	0.964%
4800 nm Cu/quartz (Fig. 5a)	149 nm	110 nm	639	2.18%
4800 nm Cu/quartz (Fig. 5b)	161 nm	117 nm	639	2.24%
1200 nm Cu/sapphire (Fig. 6a)	5.19 nm	4.20 nm	1600	0.0033%
1200 nm Cu/sapphire (Fig. 6b)	2.91 nm	2.28 nm	1600	0.0016%

S2: As-deposited and annealed Cu films

Cu films have been fabricated by electron beam evaporation of Cu pellets (Kurt J. Lesker Company, 99,999% pure) at room temperature with a base pressure of 2×10^{-7} mbar and a deposition rate of 5 Å/s. As-deposited Cu films exhibit a columnar microstructure with small crystallites as shown in Fig. 7.

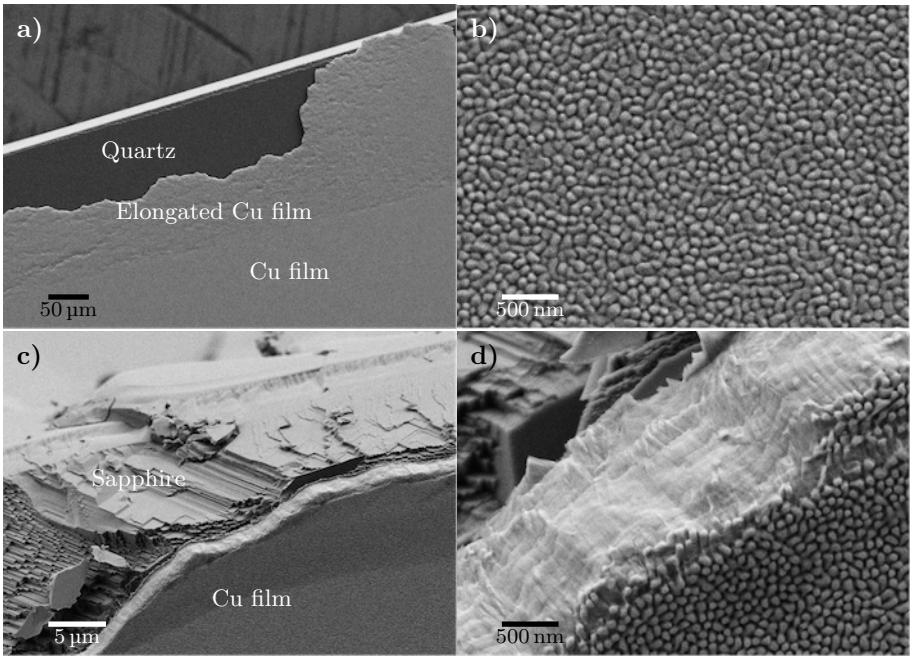

Figure 7: SEM images of a 1.2 µm-thick Cu film as-deposited on **(a-b)** a fused quartz and **(c-d)** a crystalline C-plane sapphire wafer. **(b)** and **(d)** are higher magnification images of **(a)** and **(c)**, respectively.

Annealing the Cu film pre-deposited on fused quartz results in the abnormal growth of Cu grains. Grains with Cu(111) surface orientation grow at the expense of others as observed with electron backscattering diffraction (EBSD) images (see Fig. 8).

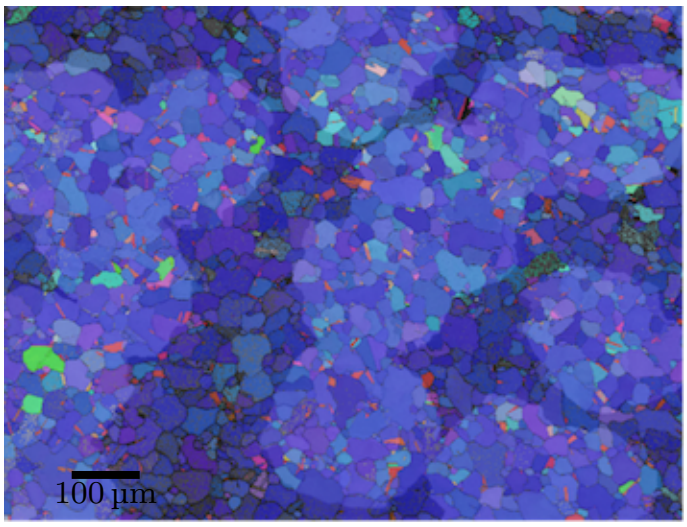

Figure 8: Electron backscattering diffraction (EBSD) image taken on a 1.2 µm-thick thin Cu film pre-deposited on a fused quartz wafer after the growth of individual graphene domains. Cu surface crystallography can be observed through graphene due to its transparency to high energy electrons (15 keV). The contrast probably stems from the fact that graphene protects the Cu surface from oxidation which disturbs the EBSD measurements. Red, green and blue colors correspond to Cu(100), Cu(101), and Cu(111), respectively.

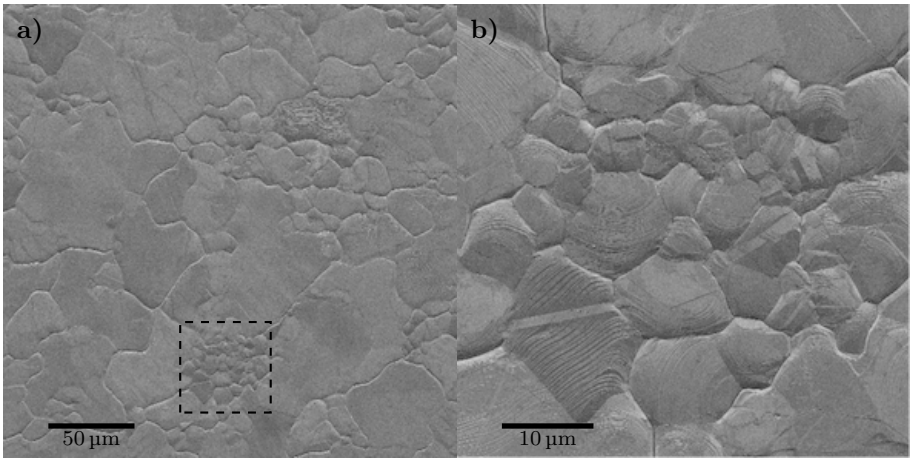

Figure 9: SEM images of the surface of 800 nm-thick Cu film after a CVD process comprising a 1 hour-long graphene growth step at 1050°C under atmospheric pressure conditions. Smaller Cu grains have a lateral size of about 3 micrometers. (b) is a higher magnification image of the surface area in the black dashed rectangle in (a).

S3: Cracks and wrinkles in graphene on Cu foil

Figure 10 shows that the cracks (white parallel lines in in-lens images) have an orientation which varies from one underlying Cu grain to another, even within a single-crystalline graphene domain. Cracks can also be directly visible using dark field optical microscopy as shown in Fig. 11.

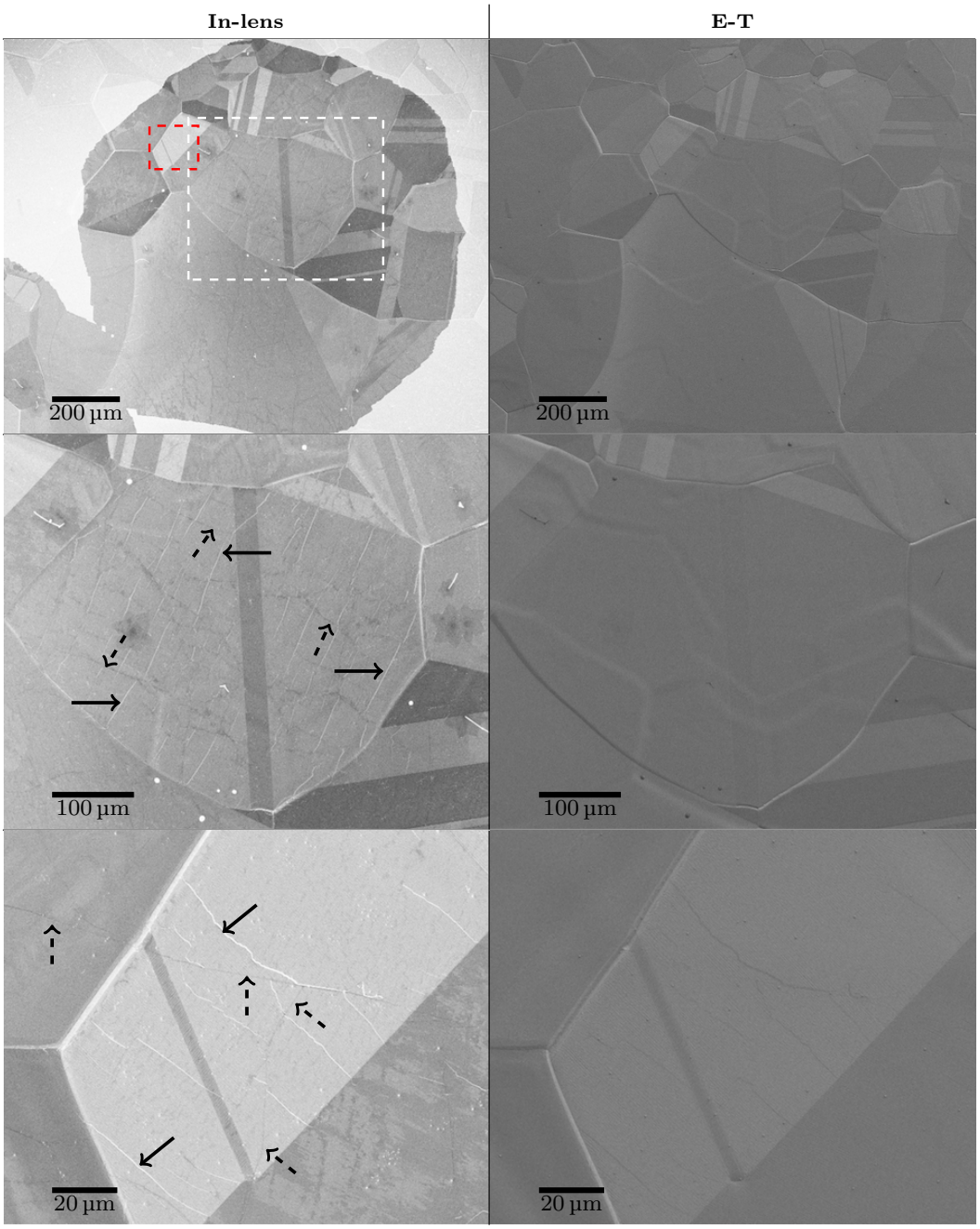

Figure 10: SEM images of a single crystal of graphene grown on a 50 µm-thick Cu foil using (left panel) in-lens detector and (right panel) regular E-T detector to observe graphene's physical integrity and the Cu surface morphology, respectively. Middle and bottom panels are higher magnification images of the surface areas in the white and red dashed rectangles in the top panel, respectively. Graphene cracks (white fine lines) and wrinkles (black finer lines) are indicated with solid and dashed black arrows in the in-lens images, respectively.

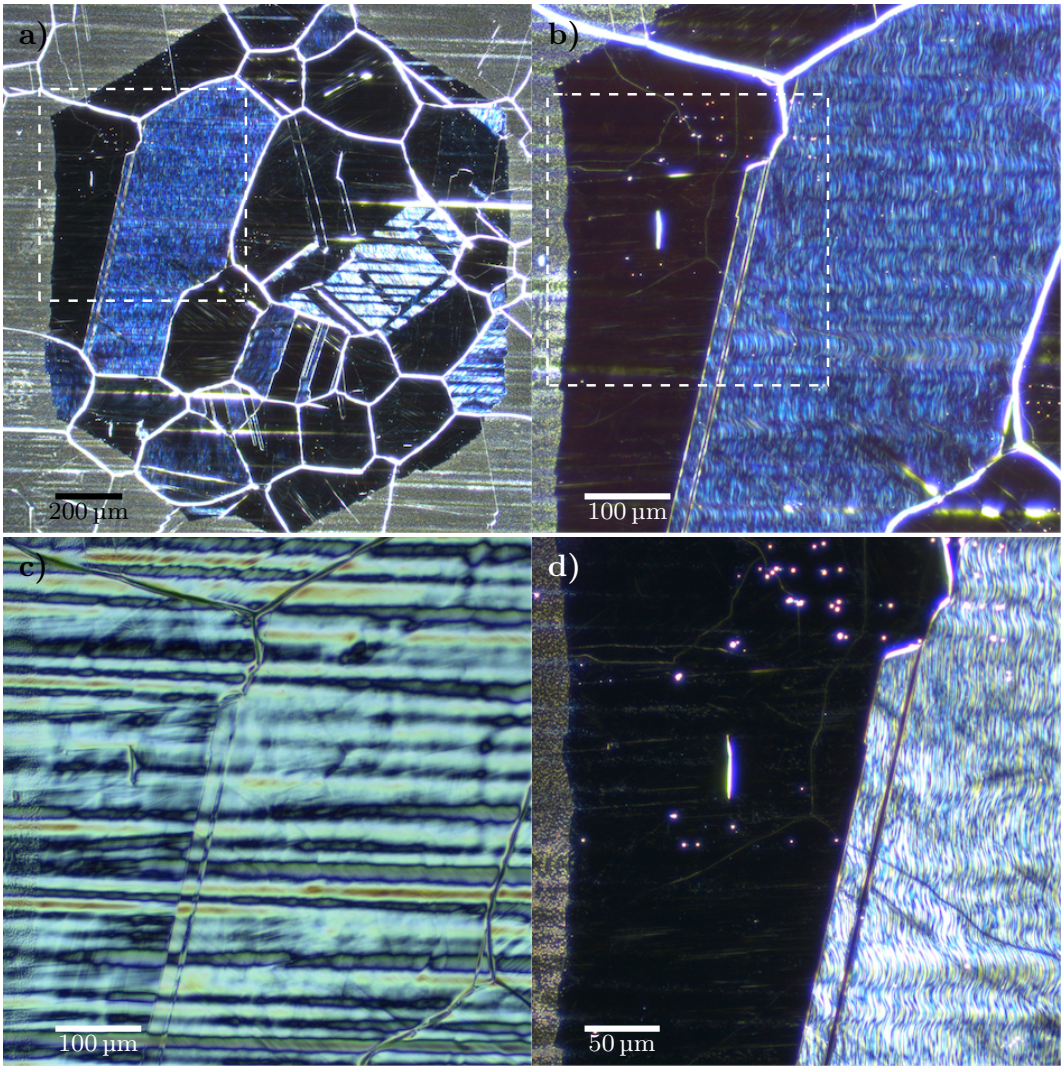

Figure 11: a) Dark field (DF) microscopy image of a graphene single crystal as grown on a Cu foil. b) higher magnification DF image of the area in the white dashed rectangle in (a). c) Bright field image of the Cu surface region shown in (b). d) Higher magnification DF image of the area in the white dashed rectangle in (b).

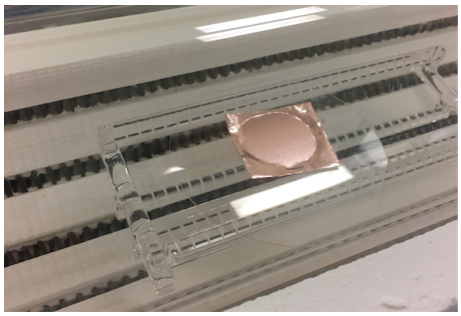

Figure 12: Photograph illustrating the Cu foil tendency to stick on the support (quartz wafer in this case) in the sample center and have its edges bending upwards when cooling down after the CVD process. The Cu foil in-situ deformation and post-CVD handling are prone to cause additional strain in graphene and contribute to the formation of cracks and wrinkles.

S4: Cracks and wrinkles in graphene on Cu films

Graphene grown on Cu/quartz

Figures 13 and 14 shows that cracks (white parallel lines in in-lens images) in graphene grown on polycrystalline Cu films tend to propagate along the Cu grain boundary grooves. Graphene grown on top of Cu films with smaller Cu grain tends to have a higher density of cracks. Figures 13 and 14 also show that graphene features no or very little wrinkles compared to graphene grown on Cu foils.

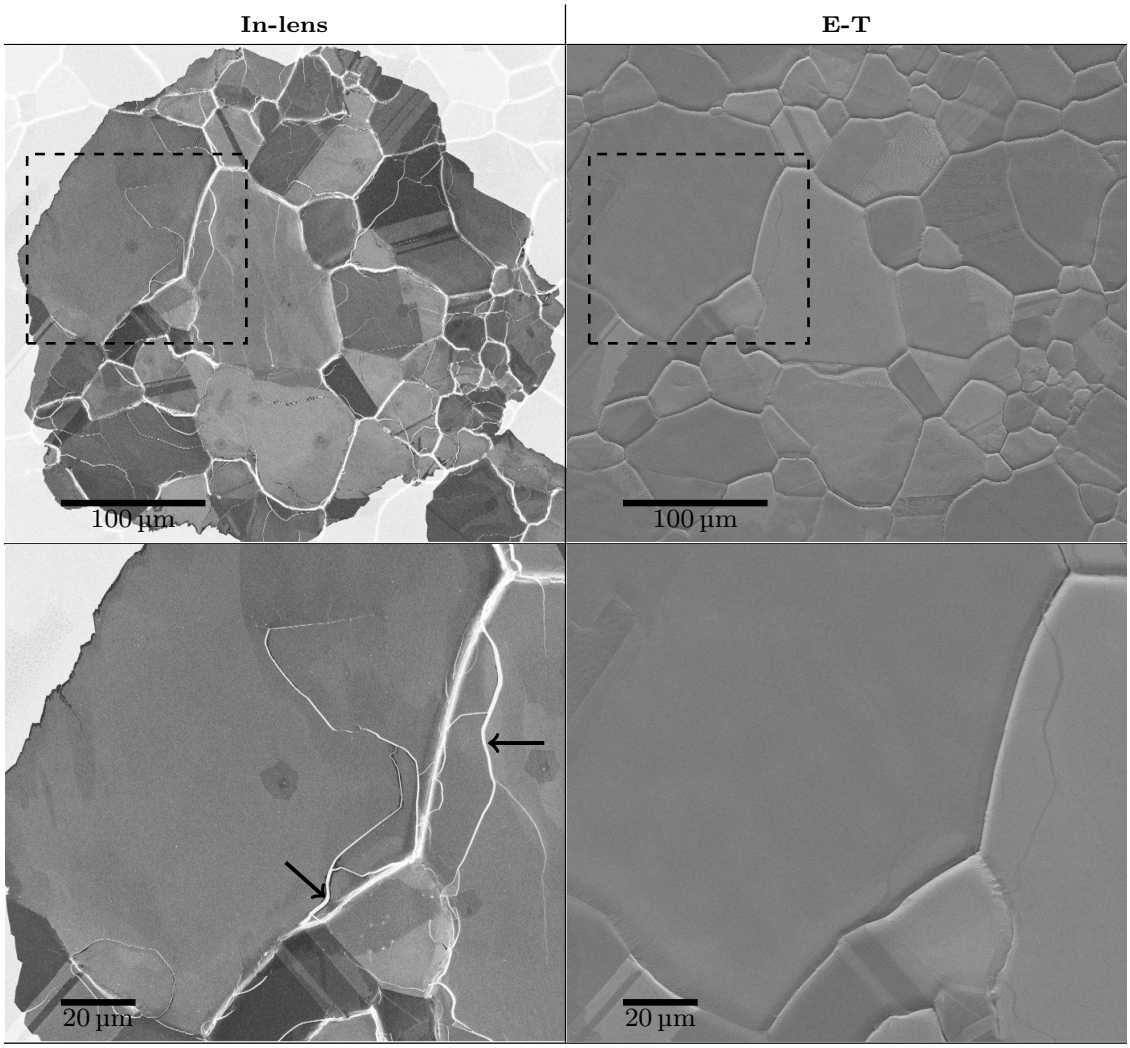

Figure 13: SEM images of a single crystal of graphene grown on a 1200 nm-thick Cu film (deposited on fused quartz) using (left panel) in-lens detector and (right panel) regular E-T detector to observe graphene's physical integrity and the Cu surface morphology, respectively. Bottom panels are higher magnification images of the surface areas in the black dashed rectangles in the top panel. Graphene cracks (white fine lines) are indicated with solid black arrows in the higher magnification in-lens image.

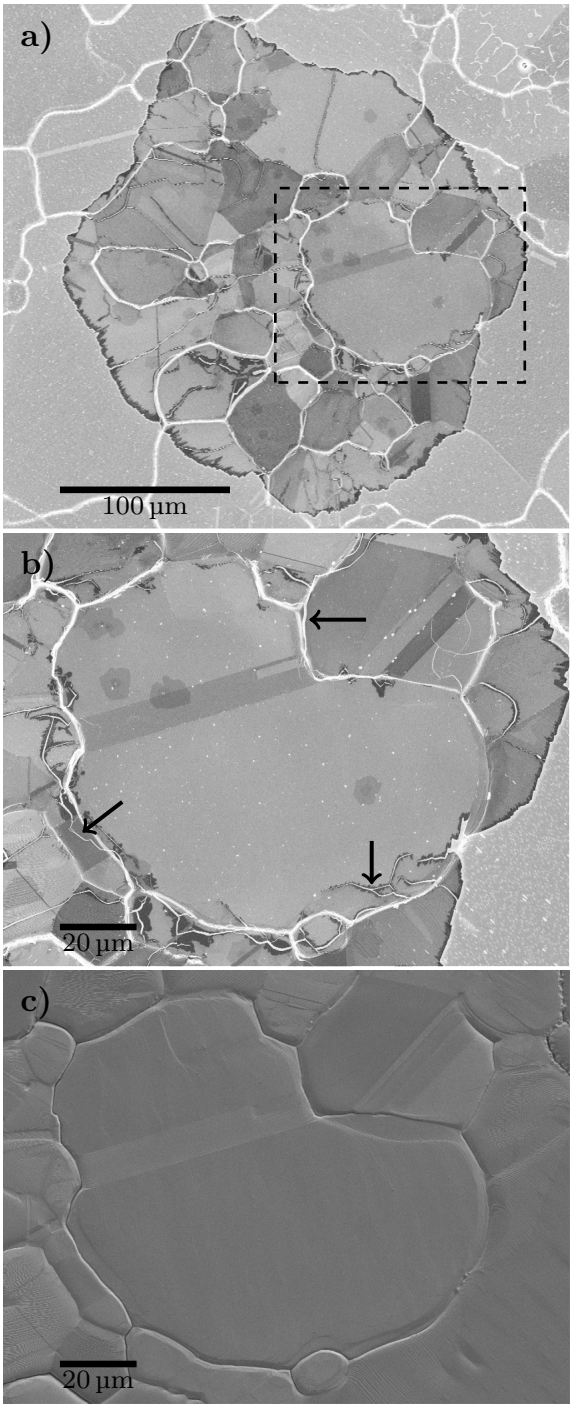

Figure 14: a) In-lens SEM image of a graphene single crystal grown on a 1200 nm-thick Cu film (deposited on fused quartz). b) Higher magnification SEM image of the area in the dashed rectangle in (a). c) E-T SEM image of (b) to visualize the underlying Cu surface microstructure. Graphene cracks are indicated with solid black arrows in (b).

Graphene grown on Cu/sapphire

Depending on the cleanliness and surface state of the Cu/sapphire interface, the Cu film can either be single crystalline or polycrystalline. In the polycrystalline Cu film on sapphire, the Cu surface orientation remains Cu(111) but the grains have different in-plane orientations. Figure 15 shows two individual graphene domains that have grown on a Cu/sapphire substrate in a transitional area between poly- and single crystalline Cu film regions. Figures 16 and 17 represent higher magnification SEM images of the single-crystalline and polycrystalline areas in Fig. 15, respectively.

As shown in Fig. 16, graphene grown in single-crystalline Cu film does not exhibit any cracks. However, high magnification in-lens SEM images reveal the presence of wrinkles (dark narrow lines). These wrinkles are made more visible by natural Cu surface oxidation which is favored in their vicinity.

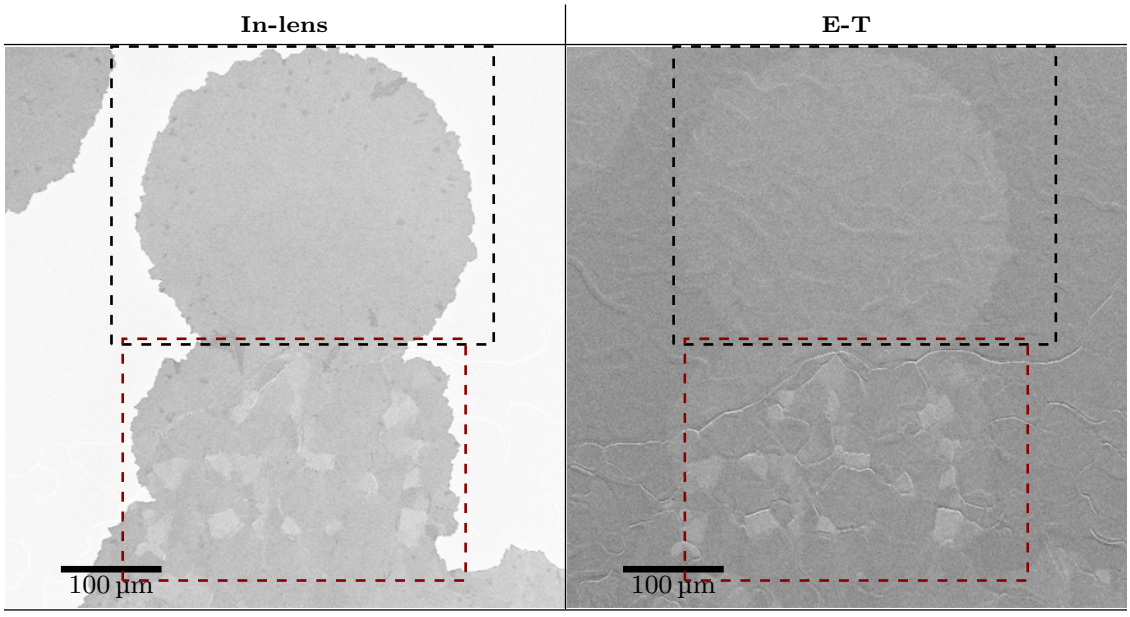

Figure 15: In-lens and E-T SEM images taken on a Cu/sapphire substrate after graphene growth. The top graphene domain has grown on single crystalline Cu film while the graphene domain at the bottom has grown on polycrystalline Cu(111) domains.

On the other hand, graphene grown on polycrystalline Cu film pre-deposited on a sapphire substrate contains both cracks and wrinkles. The dimension and density of these cracks is however significantly inferior to those that can be found on Cu/quartz substrates and Cu foils. These cracks are mostly located around Cu grain boundary with deep grooves as shown in Fig. 16.

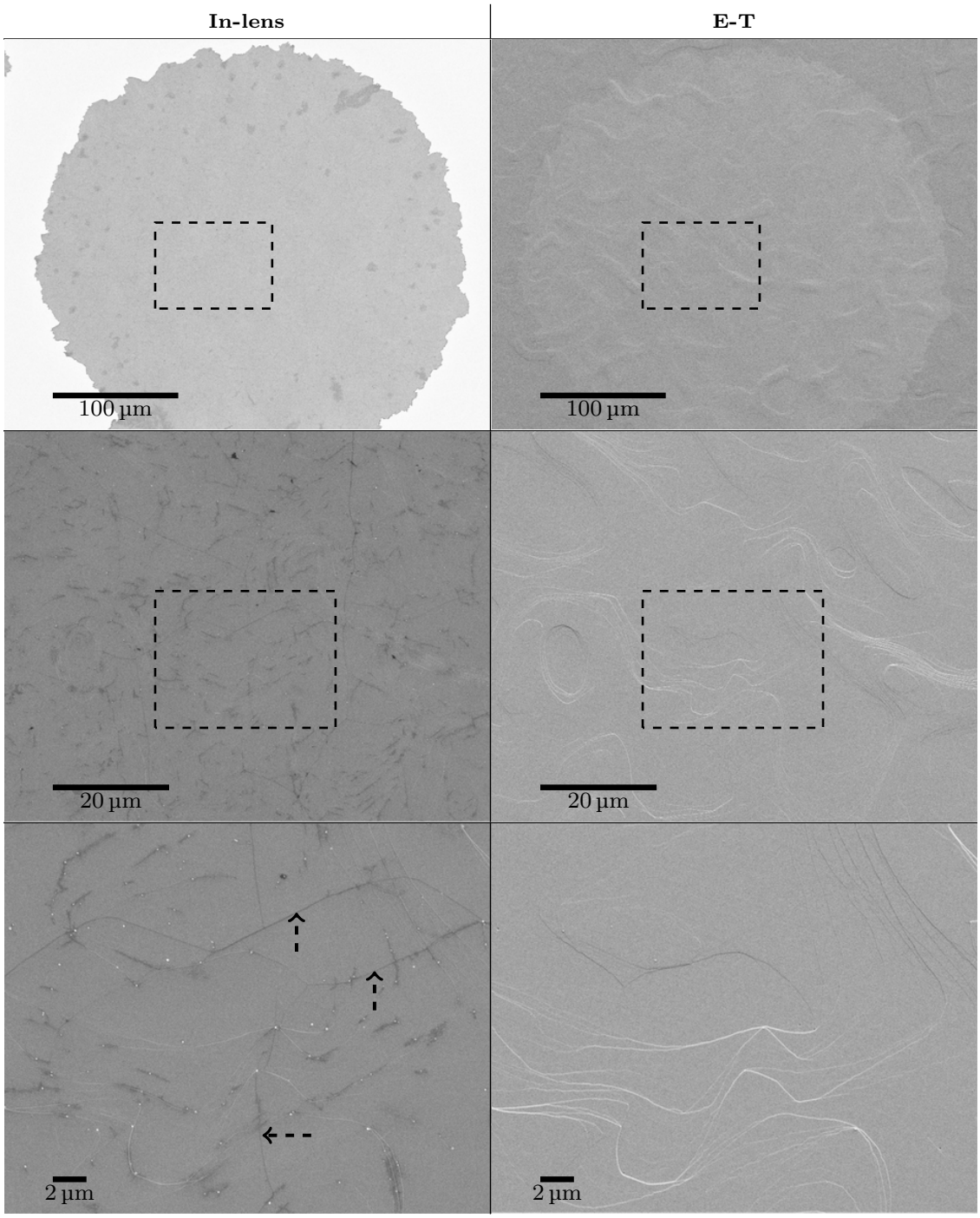

Figure 16: SEM images taken on a single crystalline Cu/sapphire region (corresponding to the back dashed rectangle in Fig. 15) after graphene growth. Middle panel is a higher magnification image of the Cu surface area in the dashed black rectangle in the top panel. Bottom panel is a higher magnification image of the Cu surface area in the dashed black rectangle in the middle panel. Graphene wrinkles (black fine lines) are indicated with dashed black arrows in the bottom panel in-lens image.

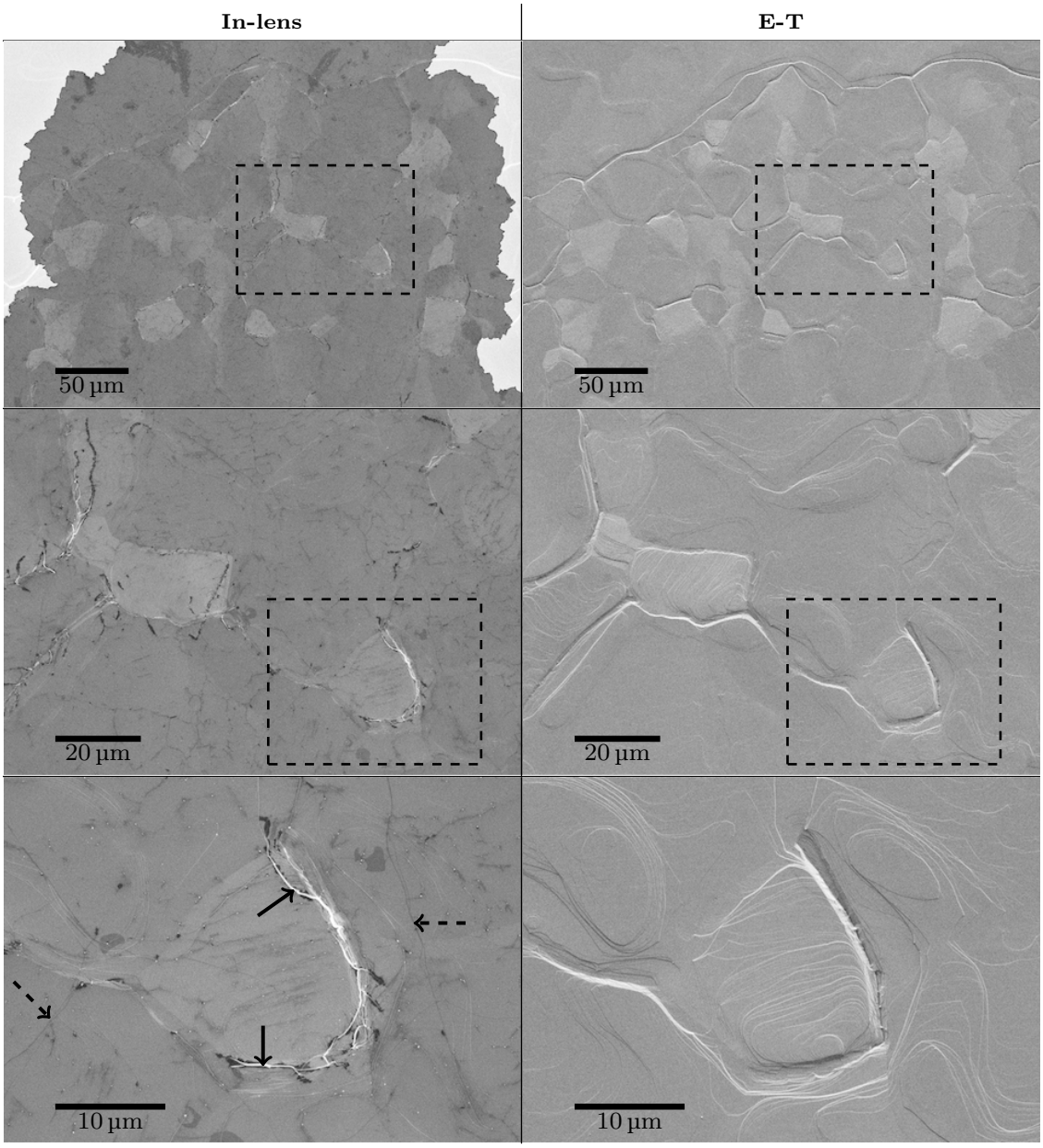

Figure 17: SEM images taken on a single crystalline Cu/sapphire region (corresponding to the back dashed rectangle in Fig. 15) after graphene growth. Middle panel is a higher magnification image of the Cu surface area in the dashed black rectangle in the top panel. Bottom panel is a higher magnification image of the Cu surface area in the dashed black rectangle in the middle panel. Graphene cracks (white fine lines) and wrinkles (black finer lines) are indicated with solid and dashed black arrows (bottom panel, in-lens image), respectively.

S5: Stressed Cu film and wafer curvature

The residual stress present in a thin Cu film deposited on a thick substrate can be determined by the Stoney formula. The calculation is based on the measurement of the curvature of the C-plane sapphire before the Cu film deposition, right after the Cu film deposition and after the CVD process. The radius of the curvature has been measured using contact profilometry with a 2.5 µm tip and a scanning length of 5.5 cm which represents about two third of the dimension of our 3 inch-wafer. In general, the total stress in the film is the sum of 3 contributions: the internal stress (σ_{int}), the stress induced by external loading (σ_{ext}), and the thermally-induced tress (σ_{therm}).

Given that no external loading is applied to the wafer in our experimental conditions, σ_{ext}=0. The internal stress σ_{int} cannot be neglected given that the bare sapphire substrate exhibits an initial curvature (see Fig. 18, top blue curves). After the Cu film deposition, the sapphire/Cu has a more pronounced curvature due to internal stress in the Cu film (see Fig. 18, bottom orange curves). This internal stress is not going to be taken into account in our calculations given that the CVD process comprises a 1 hour-long step at 1050°C, that is, about 33°C below the melting point of copper. It is very likely that such a long duration exposure to high temperature results in the vanishing of any stress present in the Cu film. Although the Cu film relaxes and conforms to the thick sapphire substrate deformation during the high temperature Cu annealing and graphene growth steps, a tensile stress builds up in the Cu film during the cooling step due to difference in the CTE between Cu and the sapphire. As graphene is an atomically thin film, its impact on the wafer curvature is neglected.

In the case of purely elastic deformation and using averaged values for the thermal expansion coefficients, a first theoretical approximation of the deformation and stress induced by the sapphire substrate on the Cu film can be calculated:

$$\epsilon_{\text{therm}} = \big(\alpha_{Cu} - \alpha_{sap}\big)\big(T_{CVD} - T_{RT}\big) \tag{1}$$

$$\epsilon_{\text{therm}} = \big(18 \times 10^{-6} - 7.8 \times 10^{-6}\big)\big(1050 - 20\big) \tag{2}$$

$$\epsilon_{\text{therm}} = 0.0105 \approx 1\% \tag{3}$$

$$\tag{4}$$

$$\sigma_{\text{therm}} = E_{Cu} \times \epsilon_{\text{therm}} \tag{5}$$

$$\sigma_{\text{therm}} = 117[GPa] \times 0.0105 \tag{6}$$

$$\sigma_{\text{therm}} = 1.23[GPa]. \tag{7}$$

Given that the stress is more likely to be equibiaxial than than uniaxial, a more accurate estimation can be calculated using:

$$\sigma_{\text{therm}} = \frac{E_{Cu}}{1 - \nu_{Cu}} \times \epsilon_{\text{therm}} \tag{8}$$

$$\sigma_{\text{therm}} = \frac{117[GPa]}{1 - 0.355} \times 0.0105 \tag{9}$$

$$\sigma_{\text{therm}} = 1.90[GPa]. \tag{10}$$

If it is assumed that the Cu film deformation is purely elastic and the sapphire wafer has no initial stress, Stoney formula can be used to determine the theoretical wafer curvature that the sapphire/Cu substrate would take after the CVD process. Using C-plane sapphire substrate Young's modulus E_{sap}=345 GPa, the Poisson's ratio ν_{sap}=0.29, and thick-

ness t_{sap}=500 µm, we obtain:

$$\sigma_{\text{therm}} = \frac{E_{sap}}{6(1-\nu_{sap})}\frac{t_{sap}^2}{t_{Cu}}\Big(\frac{1}{R_{post}} - \frac{1}{R_{pre}}\Big) \tag{11}$$

$$\sigma_{\text{therm}} = \frac{345\times10^9}{6(0.71)}\frac{(500\times10^{-6})^2}{2.4\times10^{-6}}\Big(\frac{1}{R}\Big) \tag{12}$$

$$1.9\times10^9 \approx \frac{8.44\times10^9}{R} \tag{13}$$

$$R \approx 4.44[m]. \tag{14}$$

As it can be seen in Fig. 18, the measured wafer curvature after the CVD process is around 45 m, that is, one order of magnitude larger without even taking into account the impact of the initial stress in the bare sapphire wafer. It is thus clear that the Cu film underwent plastic deformation during the cooling step of the CVD protocol.

The internal stress present into the Cu film directly after the CVD process can be determined (with initial curvature correction):

$$\sigma_{\text{Cu exp}} = \frac{E_{sap}}{6(1-\nu_{sap})}\frac{t_{sap}^2}{t_{Cu}}\Big(\frac{1}{R_{post}} - \frac{1}{R_{pre}}\Big) \tag{15}$$

$$\sigma_{\text{Cu exp}} = \frac{345\times10^9}{6(0.71)}\frac{(500\times10^{-6})^2}{2.4\times10^{-6}}\Big(\frac{1}{44.902m} - \frac{1}{62.859m}\Big) \tag{16}$$

$$\sigma_{\text{Cu exp}} \approx 8.44\times10^9\times6.36\times10^{-3} \tag{17}$$

$$\sigma_{\text{Cu exp}} \approx 5.37\times10^7[Pa] \tag{18}$$

$$\sigma_{\text{Cu exp}} \approx 0.054[GPa] \tag{19}$$

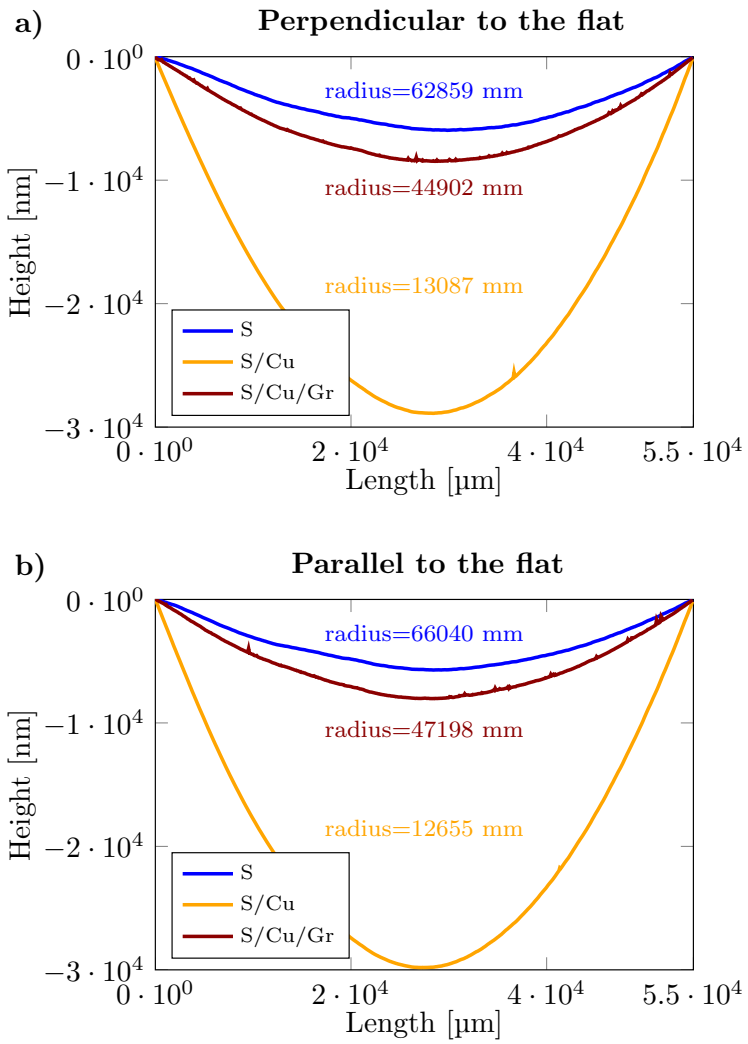

Figure 18: Wafer curvature scans acquired on a sapphire wafer as-received (top blue curves), after the deposition of a 2.4 µm-thick thin Cu film (bottom orange curves), and after the CVD process (middle red curves). 55 mm-long profilometer scans have been taken across the wafer (a) perpendicularly and (b) in parallel relatively to the flat of the wafer.

S6: Graphene grain boundaries

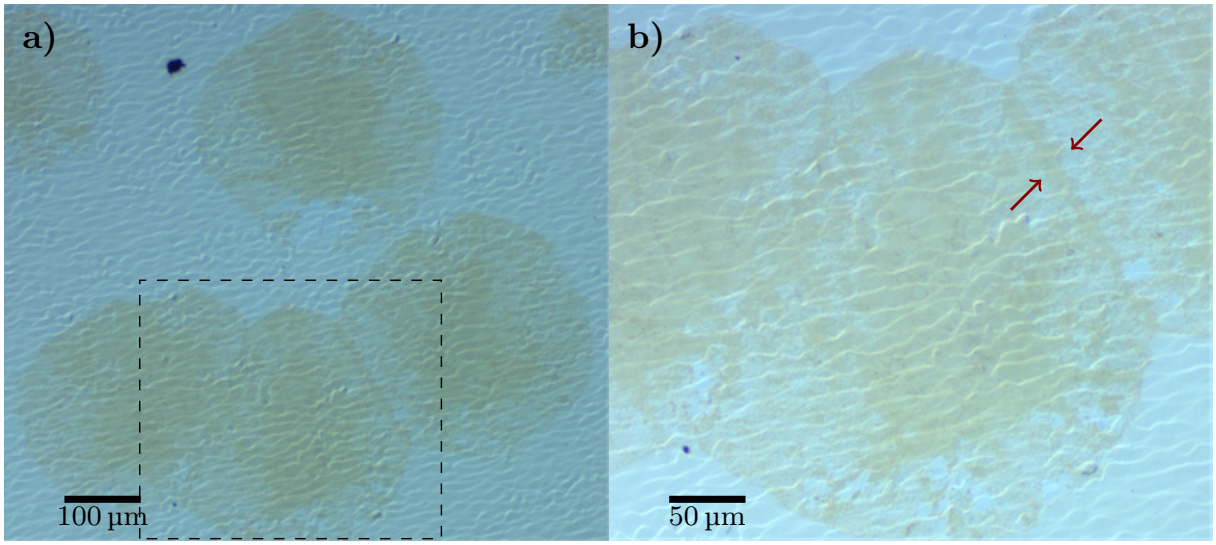

Figure 19: DIC optical images taken on the surface of an epitaxial Cu film after the growth of individual graphene domains. Graphene domains are visible due to natural oxidation occurring preferentially underneath graphene. Image (b) represents a higher magnification image of the dashed black square in (a). Red arrows in (b) show the location of a graphene grain boundary which is visible because of localized oxidation of the Cu surface underneath. Such localized oxidation suggests that the graphene grain boundary is permeable to oxygen molecules.

S7: Graphene domain density on bare Cu

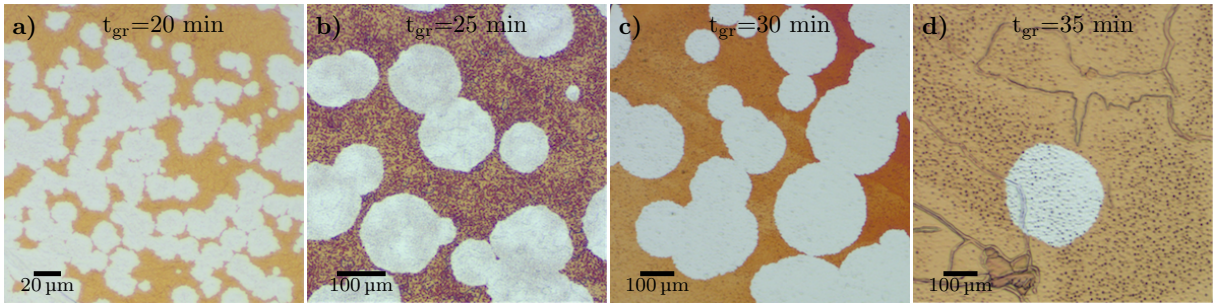

Figure 20: Optical microscope images of graphene grown on epitaxial Cu film after a slight Cu oxidation to make graphene visible. Graphene growth results in (a), (b), (c), and (d) correspond to CVD processes involving the introduction of H_2 in the CVD furnace at 750°C, 900°C, 1050°C, and after 20 min at 1050°C, respectively. In contrast to Fig. 3 of the paper, the Cu films shown here were oxidized for 2 min at 200°C in air on a hot plate before the CVD process. It can thus be observed that graphene domain shape, density and dimensions are very little or not impacted by the presence of a surface Cu oxide layer.

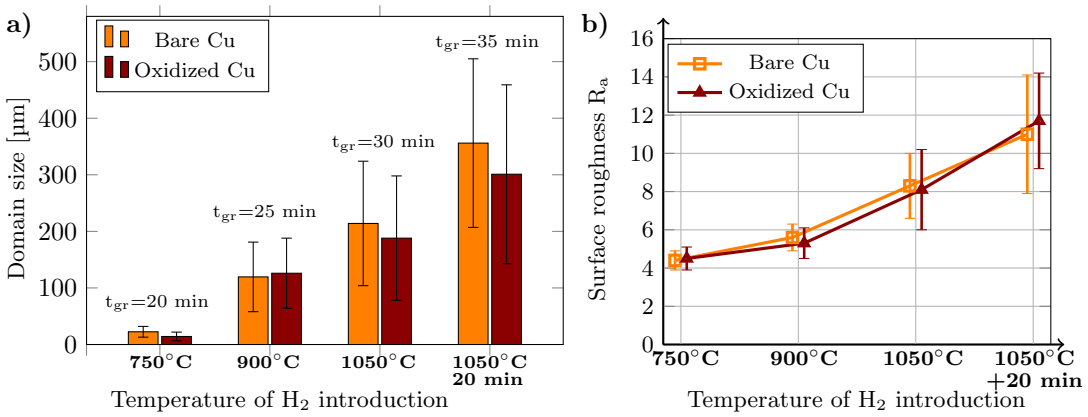

Figure 21: a) Bar chart representing the lateral size of graphene domains (on both bare and pre-oxidized epitaxial Cu films) for the CVD processes involving the introduction of H_2 in the CVD furnace at 750°C, 900°C, 1050°C, and after 20 min at 1050°C. These results suggest that pre-oxidizing the Cu film prior to the CVD process has very little or no influence on the graphene growth rate. b) Evolution of the Cu surface roughness with the temperature of introduction of H_2.

S8: Cu film oxidation, voiding and dewetting

Depending on whether the Cu film is deposited on fused quartz or C-plane sapphire wafers, the oxidation induced by the high temperature annealing in a non-reducing atmosphere differs.

Polycrystalline Cu film

On fused quartz, the traces of oxygen present in the Ar flow tend to oxidize the surface of the Cu film and create some Cu oxide grains that spread over the entire film thickness. The top Cu oxide layer is transparent to light and cannot easily be observed with optical microscopy (see Fig. 22). The Cu oxide grains reaching the underlying fused quartz surface are visible when observing the Cu surface topside as well as from the wafer backside. Indeed, as the fused quartz wafer is transparent and polished on both sides, the backside of the Cu film can be observed through the quartz wafer as shown in Fig. 23.

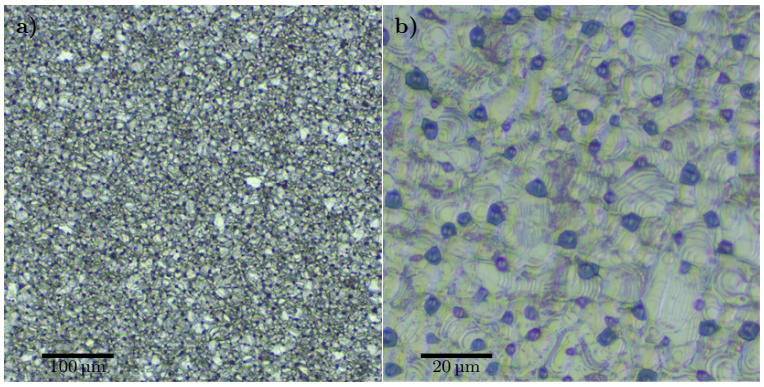

Figure 22: Optical images of a 1200 nm-thick Cu film top surface after annealing (1 hour-long heating ramp to 1050°C, 20 min-long plateau at 1050°C, 1 hour-long cooling down to room temperature) in Ar under ambient pressure conditions.

Prolonging the duration or increasing the temperature of the Cu annealing step makes the Cu surface oxide layer thicker and increase the amount of Cu oxide present at the interface with the fused quartz surface. When hydrogen is introduced for the graphene growth step, it reduces the Cu oxide into its metallic form and release water vapor. Cu film is prone to voiding and dewetting when the Cu oxide represents a too large proportion of the Cu film.

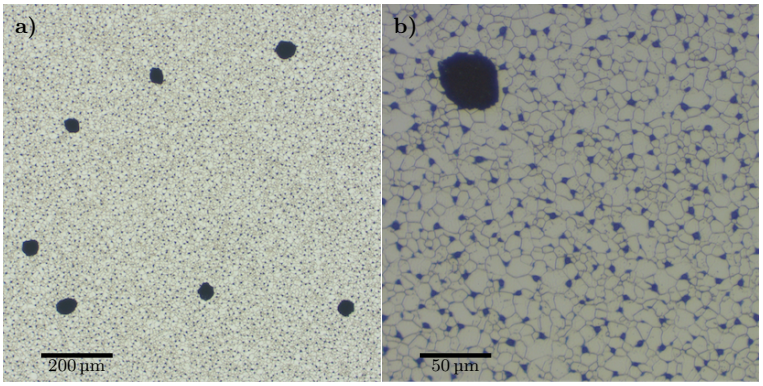

Figure 23: Optical images taken on the backside of the Cu/quartz sample presented in Fig. 22.

Reducing the reduction rate by decreasing the temperature or decreasing the rate of arrival of hydrogen on the Cu film has been found to have a beneficial effect on the Cu film physical integrity.

Epitaxial Cu film

Epitaxial Cu films do not exhibit any Cu oxide grains when annealed in a non-reducing atmosphere. The Cu oxide top layer forms crystalline triangles and very small crystallites as shown in Fig. 24. On the other hand, very little Cu oxide is present at the interface under the Cu film. The absence of penetration of oxygen deep into the Cu film probably stems from the absence of Cu grain boundary that can serve as a pathway for the diffusion of oxygen. Nevertheless, excessive oxidation of the Cu film also leads to the Cu film voiding as can be seen in Fig. 25.

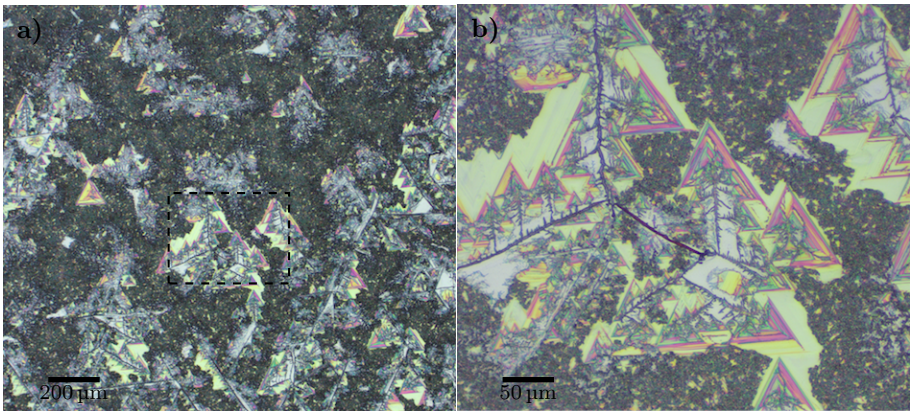

Figure 24: Optical microscope images of the Cu surface of a 1200 nm-thick epitaxial Cu film after being annealed (1 hour-long heating ramp to 1050°C, 20 min-long plateau at 1050°C, 1 hour-long cooling down to room temperature) in the CVD furnace in an argon atmosphere under ambient pressure conditions.

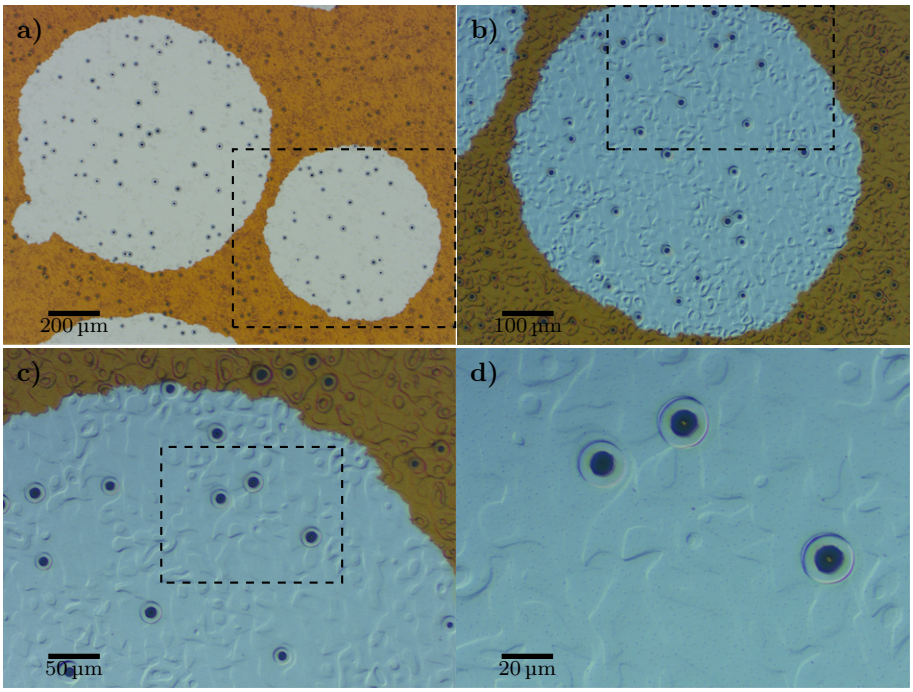

Figure 25: Optical image of graphene grown on a 1200 nm-thick epitaxial Cu that underwent excessive oxidation during the Cu annealing step.

The fact that large graphene domains (i.e. with a lateral size exceeding one millimeter) have been synthesized on such voided and rough Cu surface strongly suggests that the Cu surface roughness plays a minor role in controlling the graphene domain seeding density and consequently the graphene domain size. Therefore, the oxidative carbon removal of the Cu substrate seems to be the key factor governing the graphene seeding density.

S9: SEM images of Cu surface depressions

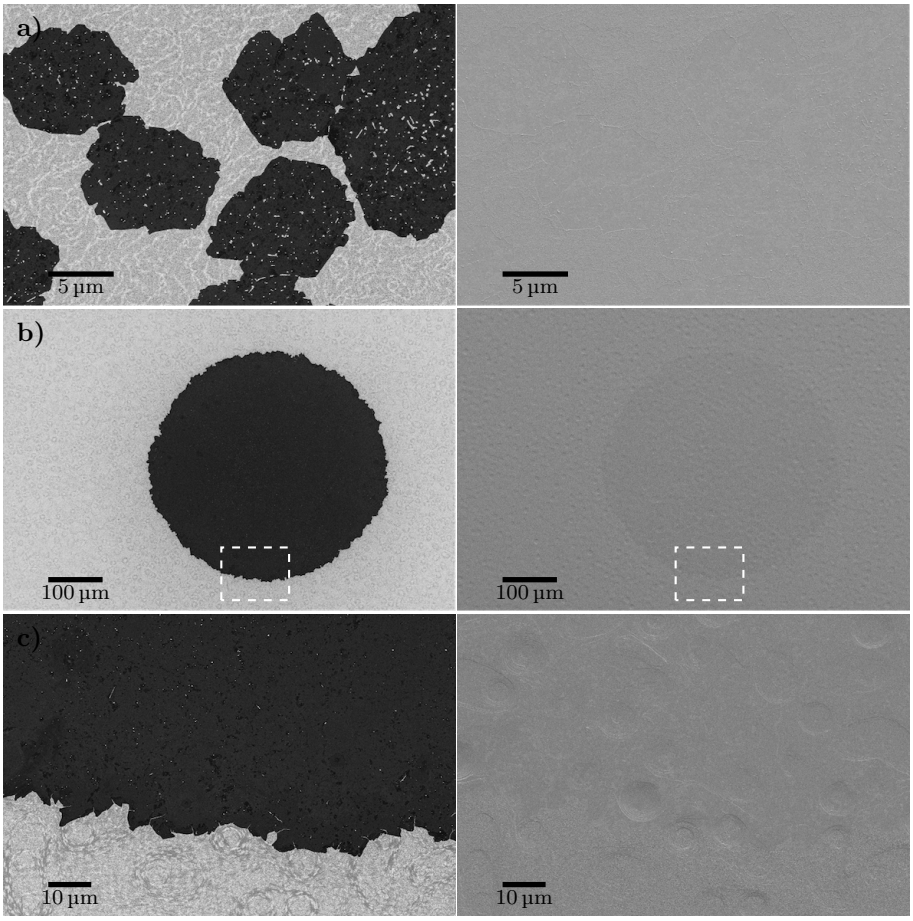

Figure 26: Scanning electron microscopy images of graphene grown on Cu/sapphire substrates. Left panel: in-lens detector to observe graphene domain shape, size and density. Right panel: regular E-T detector showing Cu surface morphology. Graphene has been grown using the CVD protocol described in Fig. 3 of the paper. a) Hydrogen has been introduced at 750°C. b) Hydrogen has been introduced after 20 min at 1050°C. c) Higher magnification images of the Cu/graphene surface presented in (b) to point out the presence of depressions.

S10: CVD protocol with mm-size graphene domains and improved surface roughness

Slowing down the rate of reduction of the Cu film upon introduction of hydrogen is key to produce large graphene domains on a Cu surface exhibiting a roughness of a few nanometers. The CVD protocols presented in Figs. 27 and 28 provide a better surface roughness (R_a in the 1.2–2.8 nm range) but a similar graphene domain density as the fast reduction protocol described in Fig. 3 of the manuscript (i.e. a density in the 0.5–2 domains/mm^2).

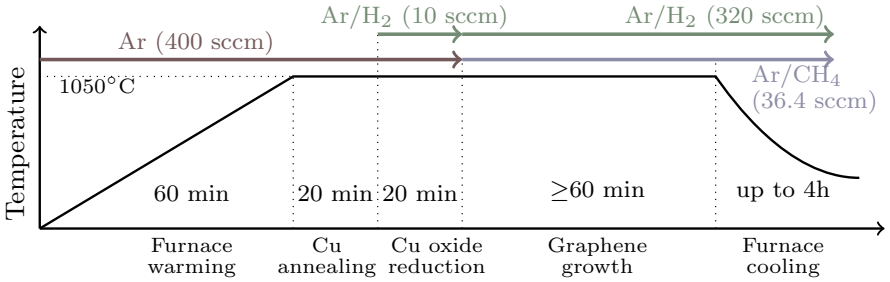

Figure 27: Temperature and gas flow rate profiles used to grow millimeter-size graphene domains on each type of substrate while mitigating the roughening effect of the oxidative carbon removal. Graphene growth results are shown in Fig. 29.

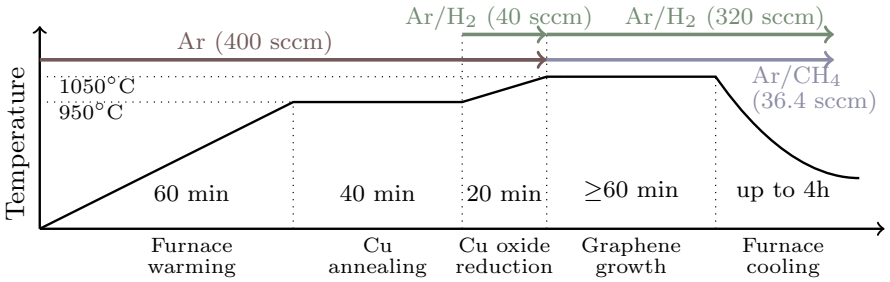

Figure 28: Temperature and gas flow rate profiles used to grow millimeter-size graphene domains on each substrate while mitigating the roughening effect of the oxidative carbon removal. This alternative protocol can be useful when the CVD apparatus is not designed to inject a very small gas flow rate of hydrogen and thus enable a slow Cu oxide reduction.

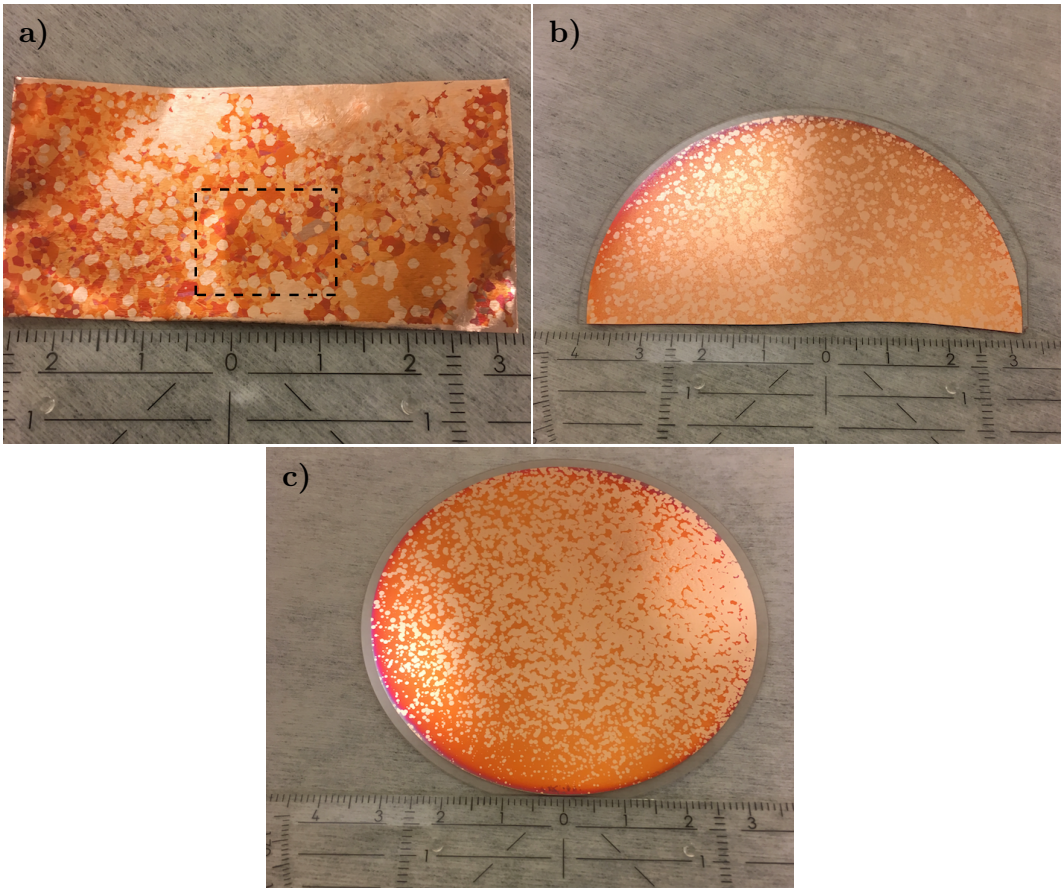

Figure 29: Photographs of the widely used Cu substrates after the graphene growth process presented in Fig. 27. The Cu surface has been slightly oxidized (on a hot plate for about 30s at 240°C) to make graphene visible. a) 50 µm-thick Cu foil. b) 1200 nm-thick Cu film evaporated on a fused quartz wafer. c) 1200 nm-thick Cu film evaporated on a C-plane sapphire substrate.

S11: Graphene transfer and additional Raman measurements

After the CVD process, graphene domains have been transferred on 300 nm-thick Si/SiO_2 substrates (thermal wet oxide). The Cu/graphene samples are coated with a PMMA layer (spin coating, 2000 rpm for 1 min, 2% PMMA in anisole) and then left to dry overnight at room temperature in air. The Cu/graphene/PMMA stack is then placed in a $FeCl_3$ bath for etching away the catalyst. In the case of Cu foils, the graphene present on the foil backside is etched away using an oxygen plasma (50 W, 2 min, P$\leq$1 mbar) prior to the Cu etching step. The foil is then deposited on the surface of the $FeCl_3$ bath which etches away a 50 micrometer-thick foil in about 40 min. In the case of thin films, the 3 inch wafers are diced into 10 x 10 millimeters samples and placed in the bottom of a watch glass. A controlled amount of $FeCl_3$ is poured into the watch glass so that the Cu film is completely immersed but the sample is only a few millimeters deep under the etchant surface. In that way, the PMMA/graphene film is going to be gradually released from the quartz/sapphire wafer and float to the surface without twisting and bending too much. Once the Cu is etched away, the graphene/PMMA stack is rinsed in at least 5 successive baths of deionized water (2 liters, left for 5 minutes in each bath before switching to the next one). The graphene/PMMA stack is then scooped with the Si/SiO_2 substrate and left to dry overnight. Once the graphene/SiO_2 interface is dry, a drop of fresh PMMA is deposited on the PMMA film in order to soften it and improve the adhesion between graphene and the underlying SiO_2 surface. Enough fresh PMMA is dropped so that it can be left for 40 min without drying. Finally, the PMMA is removed in a warm acetone bath (50°C) for 30 min. As the PMMA has not been baked after the spin coating, it conforms better to the final substrate surface morphology upon the re-deposition of fresh PMMA and it is easily removed in the acetone bath. In order to provide a more comprehensive Raman analysis, graphene has also been transferred on a hexagonal boron nitride flake pre-deposited on a 300 nm-thick Si/SiO_2 substrate. Grade A h-BN flakes (Manchester NanoMaterials) have been exfoliated using Gel-Pack films and directly transferred on the SiO_2 surface.

Raman spectroscopy mapping has been carried out on graphene as grown on copper and after transfer on both thermal silicon oxide and exfoliated h-BN flake (see Fig. 30a). Transferred graphene has been annealed for 30 min at 200°C under ambient pressure conditions in order to improve the graphene/substrate contact and potentially remove polymeric impurities/residues caused by the PMMA-assisted transfer process.

Graphene deposited on h-BN exhibits a higher $I_{2D}/_{G}$ peak intensity ratio compared with transferred on SiO_2, and an even higher compared with as-grown graphene (see Fig. 30b). This observation is in good agreement with the literature and confirms the single layer nature of graphene.[1] In the same vein, Fig. 30d shows that the 2D peak full width at half maximum is larger for as-grown graphene compared with transferred graphene which can be indicative of spatial variations of charge doping and mechanical strain.[2]

Strain and charge doping, inherently present in graphene, can be determined separately from each other owing to the strain- and doping-sensitivity of the Raman G and 2D modes.[3] Figure 30e shows the correlation between the position of the 2D and G peaks. Each data point corresponds to one Raman spectrum which corresponds to the signal average over $\sim$1 µm-wide laser spot. The dashed black lines serve as references to states of unstrained and charge-neutral graphene as reported by Lee *et al.*[3] The experimental results thus suggest that as-grown graphene exhibits a compressive strain in the 0.05-0.25% range. This strain seems to be relieved when transferred onto SiO_2 or increased when transferred onto h-BN.

While graphene transferred on h-BN seems to have very little or no charge doping, higher G peak positions values suggests a relatively strong charge transfer between as-grown graphene and the underlying Cu(111) substrate. This doping is in accordance with literature.[4]

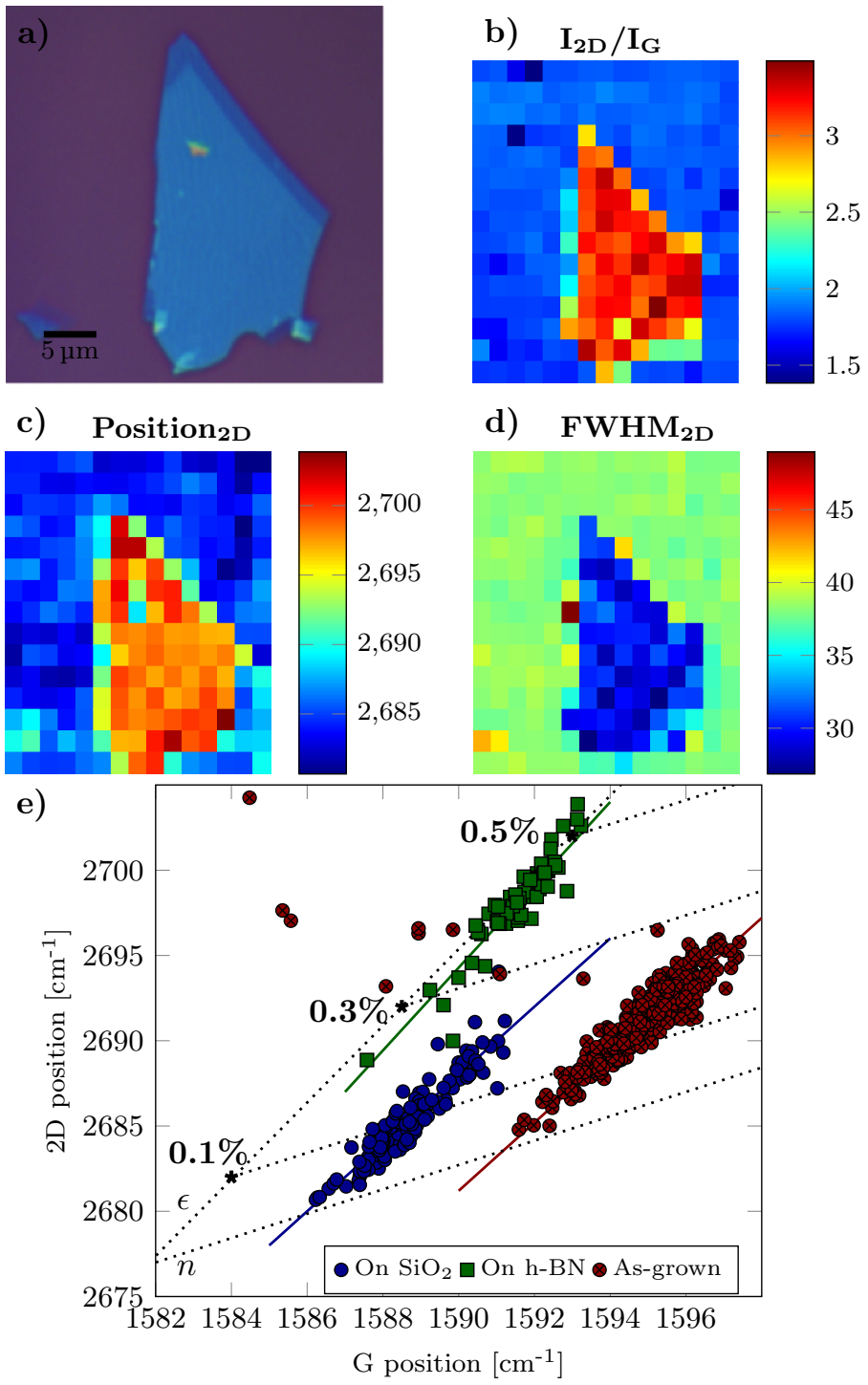

Figure 30: Complementary Raman analysis performed on graphene transferred on SiO_2 and exfoliated h-BN flake. a) Optical image of graphene on h-BN and SiO_2 used for the acquisition of Raman maps. Maps (b), (c), and (d) represent the I_{2D}/I_G intensity ratio, the 2D peak position, and the 2D peak full width at half maximum, respectively.

References

(1) Banszerus, L.; Schmitz, M.; Engels, S.; Dauber, J.; Oellers, M.; Haupt, F.; Watanabe, K.; Taniguchi, T.; Beschoten, B.; Stampfer, C. *Sci. Adv.* **2015**, *1*.

(2) Neumann, C.; Reichardt, S.; Venezuela, P.; Drögeler, M.; Banszerus, L.; Schmitz, M.; Watanabe, K.; Taniguchi, T.; Mauri, F.; Beschoten, B.; Rotkin, S. V.; Stampfer, C. *Nature Communications* **2015**, *6*, 8429.

(3) Lee, J. E.; Ahn, G.; Shim, J.; Lee, Y. S.; Ryu, S. *Nat. Com.* **2012**, *3*.

(4) Frank, O.; Vejpravova, J.; Holy, V.; Kavan, L.; Kalbac, M. *Carbon* **2014**, *68*, 440 – 451.